# A neural system for encoding odor-reward associations which influences approach behaviors

Marie A. Gadziola[1,2,3,#], Lucas A. Stetzik[1,2#], Adrianna J. Milton[3], Keiko Arakawa[3], Daniel W. Wesson[1,2,3,*]

[1]Department of Pharmacology & Therapeutics
[2]Center for Smell & Taste
University of Florida
1200 Newell Dr.
Gainesville, FL, 32610. U.S.A.

[3]Department of Neurosciences
Case Western Reserve University
2109 Adelbert Rd.
Cleveland, OH, 44106. U.S.A.

[#]Equal contributing first-authors

[*]corresponding author: danielwesson@ufl.edu (D.W.)

Running head: Valence and approach in olfaction

**Abstract**

Odors may elicit strong emotional and behavioral responses which are known to be strengthened through learning. Here we investigated how olfactory circuits transform odor information throughout their association with learned rewarded outcomes and also sought to link those neural systems with displays of reinforcement-based approach behaviors. First, we investigated the representation of odor-reward associations within two areas recipient of dense olfactory input using multi-site electrophysiological recordings and separately, fiber photometry from mice engaged in a reward-based olfactory learning task. As expected, neurons in both the posterior piriform cortex (pPCX) and olfactory tubercle (OT) represented the reward-associated valence of odors, yet both the proportion of neurons recruited by conditioned rewarded odors and the magnitudes of their recruitment were distinctly pronounced in the OT. The photometry results revealed that odor valence coding in the OT occurs among D1- but not D2-type medium spiny neurons, the principal neuron type in the OT. In both the recordings and imaging, statistically meaningful changes in activity occurred prior to instrumental behavior responses. Finally, using optogenetics we show that OT D1-MSNs influence reward-motivated approach behavior. Together our results contribute to a model whereby OT D1 MSNs support olfactory valence and ultimately hedonic-based behavioral responses.

**Key Words**

hedonics, motivation, valence, ventral striatum, olfaction

## Introduction

Upon learning, stimuli may acquire meaning, also known as valence, which is considered integral in guiding behavioral choice (Berridge and Aldridge, 2008; Chikazoe et al., 2014; Gottfried, 2009; Kumar et al., 2012; Pessoa and Adolphs, 2010; Veldhuizen et al., 2009). Learning to associate a stimulus with an outcome shapes our actions in profound manners – including impacting the choices of foods we eat and can lead to maladaptive outcomes such as those resulting from engaging in compulsive behaviors. This process enables stimuli to hold 'valence' (Lewin, 1935) which is of essence in the execution of behaviors which support satiation of basic needs (Lewin, 1935; Tolman, 1932). Despite holding fundamental importance for our day-to-day actions, the neural systems underlying the generation of valence within the brain are unresolved.

Neural signatures of valence can be observed in the form of flexible expressions of neural activity in response to stimuli throughout reward- or emotion-based associative learning (*e.g.,* (Berridge, 2019; Gore et al., 2015; Hickey and Peelen, 2015; Isosaka et al., 2015; Morrison and Salzman, 2009; Schoenbaum et al., 1998)). In mammals, this has been well established in the orbitofrontal cortex and basolateral amygdala, for instance, wherein neurons in these associative structures display differential firing following reinforcement learning for stimuli conditioned to predict a salient outcome (Roesch et al., 2007; Schoenbaum and Eichenbaum, 1995; Schoenbaum et al., 2003).

Behavioral displays linked to odor valence have been observed in all animals studied to date and involve a variety of brain systems (Knaden and Hansson, 2014; Li and Liberles, 2015). In the mammalian olfactory system, olfactory cortical structures, including both the piriform cortex (PCX) and olfactory tubercle (OT) encode the valence of odors. Specifically, work from several groups including ours (Gadziola et al., 2015; Gire et al., 2013; Roesch et al., 2007; Schoenbaum and Eichenbaum, 1995), have demonstrated that PCX and OT neurons are more greatly recruited by odors conditioned to predict rewards versus those which are unreinforced. These results have indicated that olfactory cortices encode learned odor valence by a combination of recruiting neurons into an ensemble and also divergent firing for rewarded odors.

The representation of odor valence by both PCX and OT neurons leads to the assumption that valence is a distributed, global property of the olfactory cortex. Indeed, that both PCX and OT neurons encode odor valence with divergent firing (Gadziola et al., 2015; Gire et al., 2013; Roesch et al., 2007; Schoenbaum and Eichenbaum, 1995) suggests a possible substrate wherein information within these systems is more-or-less equally relayed into downstream structures important for learning and memory (PCX; (Gottfried, 2010; Wilson and Sullivan, 2011)) or those integral for motivated and affective behaviors (OT; (Wesson and Wilson, 2011; Zhang et al.,

118 2017a)). However, this assumption is not warranted since presently no information exists
119 regarding whether either of these structures are more specialized in their capacity to encode odor
120 valence. As a specific void, no investigations of these structures simultaneously during valence
121 learning exist. Thus, an alternative system may be in place: that olfactory cortices differentially
122 represent odor valence in manners suggesting that one structure is specialized in valence
123 assignment functions. Determining whether valence is a global property distributed among the
124 PCX and OT is an important question in the overall goal of resolving the neural circuitry underlying
125 olfactory valence.

126 Based upon the representation of learned odor valence in the OT (Gadziola et al., 2015;
127 Murata et al., 2015), and the positioning of the OT within the ventral striatum (Heimer et al., 1982;
128 De Olmos and Heimer, 1999) wherein it receives dense innervation from dopaminergic neurons
129 in the ventral tegmental area (Ikemoto, 2007; Voorn et al., 1986), we predicted that the OT is a
130 central figure in assigning odors with valence. Infusion of psychoactive substances into the OT is
131 reinforcing, and rodents more robustly seek infusions into the OT than even into the nucleus
132 accumbens (Ikemoto, 2003) – highlighting the likely importance of OT dopamine in guiding
133 approach behavior, as also indicated by a recent optogenetic study (Zhang et al., 2017b). An
134 additional feature of the OT which supports this hypothesis is its cellular composition. The OT is
135 primarily composed of medium spiny neurons expressing either the D1- or D2-type dopamine
136 receptor (Murata et al., 2015). D1 MSNs in many striatal structures are activated by appetitive
137 stimuli and are often considered integral for promoting stimulus reward and approach, whereas
138 at least some reports indicate D2-type MSNs are less shaped by reinforcement (for reviews (Lobo
139 and Nestler, 2011; Soares-Cunha et al., 2016). Therefore, it is possible that previous reports of
140 neuromodulation driving reinforcement through the OT is due to direct actions upon OT D1-type
141 MSNs. Supporting this hypothesis, c-Fos expression is elevated in OT D1-type MSNs following
142 associative learning (Murata et al., 2015). Based upon the above, we predicted that OT D1-type
143 MSNs may underlie odor valence representations in the OT and separately, should therefore also
144 be capable of promoting reward-motivated approach behaviors, similar to that needed to subserve
145 engagement with odors.

146 Here we tested the above hypotheses through a combination of multi-site single-unit
147 recordings, cell type-specific fiber photometry, and cell type-specific optogenetic studies, all in
148 mice engaged in reward-motivated operant tasks. All together our results contribute to a model
149 whereby the OT, and specifically OT D1 MSNs support olfactory hedonics and ultimately hedonic-
150 based behavioral responses.

151

## Results

*Compared to pPCX, neurons in the OT robustly encode valence.*

We began by examining whether valence is a global property distributed among the pPCX and OT. We simultaneously monitored OT and posterior PCX (pPCX) single-unit activity from 11 mice implanted with chronic electrode arrays (**Fig 1 & S1A**) while they engaged in a head-fixed odor discrimination task requiring them to lick a spout for a palatable reinforcer available at the offset of conditioned-rewarded but not unrewarded odors (**Fig 1B&C**). This head-fixed paradigm allows odor-guided behaviors while maintaining precision in odor-delivery (Verhagen et al., 2007). To optimize the data contributed from each animal, all mice were shaped to discriminate between 2-4 odor pairs (Methods). Further, by excluding trials wherein animals prematurely licked during the odor we can reduce influences of motor planning or execution on the neural analyses. Baseline and odor-evoked activity were measured for isolated single neurons. The baseline firing rates of OT (median rate: 3.1 Hz; range = 0 - 56.9 Hz) and pPCX neurons (median rate: 2.1 Hz; range = 0 - 35.6 Hz) were low across the sampled population (**Fig S1B**, measured 2s prior to odor onset). In both structures, odor-evoked firing was observed in response to the odors and occurred soon after odor onset (0.35 ± 0.31s [OT], 0.57 ± 0.48s [pPCX], **Fig 1D**).

After mice learned to discriminate between odor pairs (**Fig S1C**) we observed that the majority of OT neurons were significantly modulated in their firing during the task window (65%, 52/80 OT neurons 'task-responsive' within 7s of odor onset). This was comparable to the population of pPCX neurons modulated in the same time ($X^2(df=1, n=87) = 3.32$, $p>0.05$; 44%, 35/79 neurons). To characterize responses across these populations, we measured the temporal response profile of each neuron-odor pair during correct trials by quantifying changes in firing rate from baseline using a sliding receiver operating characteristic (ROC) analysis (Cohen et al., 2012; Gadziola et al., 2015; Veit and Nieder, 2013). Area under the ROC curve (auROC) values greater than 0.5 indicate increases (excitation) in firing rate compared to baseline, with values under 0.5 indicating decreases (suppression). This analysis revealed that 91% (189/208) of OT neuron-odor pairs and 78% (110/140) of pPCX neuron-odor pairs displayed significant stimulus-evoked activity during odor presentation, with significant changes in firing rate observed shortly (<500 ms) after odor onset. Of these responses, 71% of OT and 59% of pPCX neurons increased their firing rate relative to baseline, with the remaining neurons suppressing their firing rates relative to baseline.

Across the population of neurons from both regions, we observed that OT neurons displayed more divergent responses to the conditioned odors than pPCX neurons, with more

184 robust and longer-lasting responses to conditioned rewarded than unrewarded odors (**Fig 2**). To
185 test whether the populations of OT and pPCX neurons preferentially encode one conditioned odor
186 over the other, we averaged the auROC values computed across the first 500-ms following odor
187 onset. OT neurons preferentially responded to rewarded odor with higher firing than the
188 unrewarded odors (0.59 ± 0.02 vs 0.55 ± 0.01, respectively; paired *t* test: $t_{(103)} = -6.05$, $p <$
189 $0.0001$), whereas pPCX neurons did not respond differentially to rewarded and unrewarded odors
190 across the population (0.53 ± 0.01 vs 0.53 ± 0.01, respectively; paired *t* test: $t_{(69)} = -0.73$, $p =$
191 $0.47$). Furthermore, average auROC values in response to rewarded odors were greater for the
192 population of OT neurons when compared to pPCX neurons (0.59 ± 0.02 vs 0.53 ± 0.01,
193 respectively; two-sample *t* test: $t_{(172)} = -3.49$, $p < 0.001$). There were no discernable differences in
194 the temporal response pattern of neurons that increased vs decreased firing rates, suggesting
195 that these neurons are similarly driven by conditioned odors (**Fig S2**). Next, we compared the
196 duration of significant auROC responses in the first 500ms after odor onset across the population
197 of neurons in both regions (including units with ≥ 1 significant bin). OT responses were
198 significantly longer in duration compared to pPCX responses (209 ± 97 vs 166 ± 91 ms,
199 respectively; two-sample *t* test: $t_{(290)} = -3.64$, $p < 0.001$). In addition, OT response durations to
200 rewarded odors were longer than unrewarded odors (225 ± 94 vs 193 ± 98 ms, respectively;
201 paired *t* test: $t_{(96)} = -12.01$, $p < 0.0001$), and longer than pPCX responses to rewarded odors (225
202 ± 94 vs 167 ± 84 ms, respectively; two-sample *t* test: $t_{(141)} = -3.51$, $p < 0.0001$). These results
203 support the conclusion that the representation of odor valence is not equally distributed among
204 the OT and pPCX – with the OT dominating in assigning valence.
205

206 *OT D1-type MSNs display divergent responses to conditioned rewarded odors.*

207 Which neurons are responsible for the pronounced display of valence in the OT? We
208 addressed this question by performing fiber photometry-based imaging (*e.g.,* (Gunaydin et al.,
209 2014; Kudo et al., 1992)) of GCaMP6f (Chen et al., 2013) from D1 and D2 MSNs in the OT – the
210 prominent cell populations in the OT. Mice expressing Cre-recombinase in either MSNs
211 expressing the D1 receptor (D1-Cre) or D2 receptor (D2-Cre) (Gong et al., 2003) were injected
212 with floxed GCaMP6f into their OT and later implanted with optical fibers (see Methods) before
213 being water deprived and shaped in the same lick/no-lick odor discrimination task used above.
214 During imaging (**Fig 3A & B**), the GCaMP6f emission spectrum was collected as a measure of
215 aggregate OT D1 or D2 neuron activity. Simultaneously, we also collected endogenous UV

emission spectrum as a control measure for movement artifacts. The resultant GCaMP6f signal was subtracted from the UV signal for a single output, which is considered closely reflective of aggregate neural activity.

We imaged 5 D1- and 5 D2-Cre mice with fiber implants and GCaMP6f expression both confirmed in the OT (**Fig S3**) throughout learning and performance in the lick/no-lick odor discrimination task. To enhance each animal's contributions for a more rigorous data set, we shaped each mouse on several odor pairs over differing daily sessions, yet only one pair of odors in a given session. This allowed each animal to contribute odor-modulated GCaMP6f signals to 2-3 rewarded and unrewarded odors (on different sessions) at or above criterion performance (mean rewarded odor trials / session = 44.5 [24-75 min-max range]; mean unrewarded odor trials / session = 91.3 [52-133 min-max range]). Across all rewarded and unrewarded odors, we observed modulations in both D1 and D2 MSN activity following odor onset. This was evident both looking within individual mice at subsets of trials (**Fig 3C & D**), and averaged across mice over several sessions (**Fig 3E & F**). No discernable differences were observed in the time prior to odor onset, or before 0.5s following odor onset between any stimulus type in either D1 or D2 mice (**Fig 3E & F**). Later during the odor period however (0.5-0.75s), across all D1 mice, conditioned rewarded and unrewarded odors elicited differing amounts of activity ($p<0.001$; **Fig 3E**). Whereas D1 neurons were largely unmodulated by the conditioned unrewarded odor, conditioned rewarded odors elicited large increases in activity during the odor. In contrast, no differential representation of conditioned rewarded versus unrewarded odors was observed in D2 mice, with both conditioned stimuli eliciting similar increases in activity during odor ($p=0.483$; **Fig 3F**).

*The responses of OT D1-type MSNs are flexible and encode the associated outcomes of odors.*

Having imaged D1 and D2-type OT MSNs and observing that they differently encode odor-reward associations, we were next able to ask whether this differential representation of conditioned rewarded odors observed among the D1 neuron population is flexible. In other words, does the representation of conditioned-rewarded odors flexibly follow as odors are associated to predict new outcomes? To address this, in a separate behavioral session we used reversal learning to reverse the odor-outcome contingencies so that a previously rewarded odor is no longer rewarded and a previously unrewarded odor is now rewarded. Most mice were shaped

247 upon at least 2 odor-reversals (differing odor pairs, range 2-3). If a population of MSNs is 'identity'
248 encoding they should exhibit the same odor selectivity before and after reversal learning, whereas
249 a population encoding the associative valence of an odor (rewarded or not) should reverse its
250 odor preference (Gire et al., 2013; Roesch et al., 2007). Animals took several sessions to learn
251 the reversal to criterion in this task requiring them to withhold licking until odor offset, and
252 comparisons were made only from sessions following task acquisition, during blocks consisting
253 of criterion-level performance, and correct responses during each trial.

254 On average across animals, the evoked GCaMP6f signals in D1-Cre mice tracked the
255 behavioral contingencies – with the original rewarded odor and the newly rewarded odor eliciting
256 evoked responses with similar amplitudes ($p$=0.202; **Fig. 3G**). Likewise, the original unrewarded
257 odors elicited similar responses as the new unrewarded odors ($p$=0.177). In contrast, no effect of
258 reversal on either the rewarded ($p$=0.785) or unrewarded odors ($p$=0.522) were observed in the
259 D2-Cre mice (**Fig. 3H**). D2 neurons maintained somewhat positive responses for all odors,
260 regardless of valence, indicating that while these neurons are modulated by odor, they do not
261 represent odor valence. These data support our hypothesis that OT MSNs, specifically D1-type
262 MSNs, are responsible for the profound representation of odor valence in the OT.

263

264 *OT D1 MSNs drive robust approach behaviors.*

265 Having observed reward-associated odor valence coding in OT D1, but not D2 MSNs, we
266 next asked whether the activity of these neurons directly influences the occurrence of approach
267 behaviors. Indeed, the latency and robustness of D1-MSN encoding of conditioned rewarded
268 odors may serve as an effective way whereby to activate approach behaviors. To test this, D1-
269 Cre mice injected with a floxed AAV encoding channelrhodopsin (ChR2) [n = 7] (or floxed AAV
270 encoding a reporter fluorophore [n = 5]) into their ventral striatum were later implanted with an
271 unilateral optical fiber into their OT (**Fig 4A and S4**). Mice were shaped in an optical intra-cranial
272 self-stimulation task, adapted from (Carlezon and Chartoff, 2007; Ilango et al., 2014; Vicente et
273 al., 2016), allowing for assaying of stimulation-seeking goal-directed behaviors (**Fig 4B**). Shaping
274 in this instrumental task occurred over several phases (See Methods). In the first phase, mice
275 could poke their snout into either of two ports in exchange for blue light stimulation into their OT
276 (25Hz, for 2s). All but one of the D1-Cre mice injected with AAV.ChR2 reached a level of criterion
277 performance (40 pokes into either port during a 1 hr session)(**Fig 4C**), indicating that they readily

278 learned to poke in exchange for blue light stimulation. No control AAV injected mice reached
279 criterion performance (**Fig 4C**). The mice reaching criterion on Phase 1 then progressed onto
280 Phase 2 wherein only one of the two ports delivered light. The port receiving the greater number
281 of pokes during Phase 1 was selected as the 'active' port for Phase 2. The vast majority of
282 AAV.ChR2 mice (5/6) reached criterion on Phase 2, with some poking over 500 times in the single
283 hour of testing (**Fig 4Di & ii**). To ensure that these mice were indeed seeking light stimulation, on
284 the subsequent Phase 3, the location of the active port was reversed and despite this, all the mice
285 who reached criterion on Phase 2 redirected their responding for the new active port. Compared
286 to the first session of reversal phase testing, there were significant more pokes for the active port
287 during both the last session of phase 2 testing ($p$=0.0002), as well as during the last session of
288 reversal ($p$=0.0004). These results indicate that OT D1-MSNs support behavioral approach,
289 specifically by signaling reinforcement.

290

291 **Discussion**

292 The olfactory system holds a remarkable capacity for experience-based plasticity and informing
293 a wide-range of critical behaviors. Here we build off of previous studies which have uncovered
294 odor-reward association based plasticity among neurons in both the PCX and OT (in separate
295 studies; (Calu et al., 2007; Gadziola et al., 2015; Gire et al., 2013)) to interrogate the respective
296 roles of each of these structures in the representation of odor valence by means of simultaneous
297 single-unit recordings. After identifying robust odor valence coding among neurons in the OT
298 significantly more-so than those in the PCX, we employed fiber photometry in D1-Cre and D2-Cre
299 mice to uncover evidence indicating that OT D1-, but not D2-type neurons encode odor valence.
300 Finally, we linked the activity of OT D1 neurons to the display of reward-driven behaviors,
301 specifically nose-poke based approach behaviors.

302 This work adds to a growing body of literature seeking to understand the brain systems
303 governing the generation of stimulus hedonics and preferences (for review (Berridge and
304 Kringelbach, 2015)). Attraction to odors is well established and may employ innate (unlearned) or
305 acquired (learned) mechanisms. Since the olfactory bulb is the starting-point for odor perception,
306 it is not surprising that the olfactory bulb holds importance for both innate and learned odor
307 hedonics (*e.g.,* (Doucette et al., 2011; Kermen et al., 2016; Kobayakawa et al., 2007; Wilson et
308 al., 1987). Indeed, recent work uncovered evidence that a specific zone within the main olfactory

309 bulb is necessary for generating odor hedonics (Kermen et al., 2016). The hedonic information of
310 odors in the OB next may be distributed into the OT and PCX. Both PCX and OT neurons may
311 be recruited to encode odor valence and do so with divergent firing to conditioned rewarded
312 versus unrewarded odors (Gadziola et al., 2015; Gire et al., 2013; Roesch et al., 2007;
313 Schoenbaum and Eichenbaum, 1995). A key prediction in this work was that OT units would more
314 greatly represent odor valence than those in the PCX. That said, it is quite surprising the
315 magnitude at which we found this occurs. OT units far surpassed the size of the population of
316 pPCX units encoding valence and also surpassed pPCX units in their magnitude of firing for
317 conditioned rewarded odors. Thus, through simultaneous recordings in behaving mice, this work
318 uncovers that systems downstream from the OB are specialized in their representation of odor
319 valence. This outcome is consistent with our hypothesis and also that of other groups (Kermen et
320 al., 2016).

321 Specific cell populations in several brain regions have been linked to stimulus valence or
322 to approach responses (Betley et al., 2015; Kim et al., 2019; Li and Liberles, 2015; Li et al., 2019;
323 Miller et al., 2019; Soares-Cunha et al., 2016). This work adds D1-MSNs in an underappreciated
324 ventral striatum structure, the OT, to this list and suggests a model wherein OT D1-MSNs may
325 influence downstream systems which also shape approach like the amygdala or hypothalamic
326 nuclei. This would be potentially powerful in cases wherein odors associated with positive
327 outcomes, which as we show here are represented in OT D1-MSNs, could influence downstream
328 limbic systems to strengthen approach responding through their coordinated output. All together
329 these results support a role for OT D1 neurons, not unlike D1 neurons in the nucleus accumbens
330 (Lobo and Nestler, 2011), in behaviors integral for valence -- reinforcement and stimulus-seeking.
331 It is tempting to speculate on the circuitry downstream of OT D1 MSNs which may translate
332 valence encoding or the approach behavior phenomenon we uncovered into behavior. This is a
333 highly relevant issue, especially given the broad connectivity of OT D1 MSNs through the brain's
334 affective and sensory centers (Zhang et al., 2017a).

335 Taken together, our results contribute to a model whereby the OT is a specialized center
336 for encoding odor valence. This along with the finding that OT D1-type MSNs encode olfactory
337 valence and robustly motivate reinforcement-seeking in nose-poke based task which emulates
338 snout-directed investigation behaviors like those used by rodents to sample odors, leads us to
339 predict that OT D1-type MSNs are a fundamental component of brain systems needed to inform
340 and respond to the hedonics of odors.

**Acknowledgements:** This work was supported by NIH NIDCD grants R01DC014443 and R01DC016519 to D.W. Some mouse strains used in this research were obtained from the Mutant Mouse Regional Resource Center (MMRRC), an NIH funded strain repository, and were donated to the MMRRC by the MMRRC facility at the University of California, Davis.

**Author Contributions:** Conceptualization: M.A.G., L.A.S., D.W.W.; Methodology: M.A.G., L.A.S., D.W.W.; Investigation: M.A.G., L.A.S., A.J.M., K.A., D.W.W.; Writing – Original Draft: M.A.G., L.A.S., D.W.W.; Writing – Review & Editing: M.A.G., L.A.S., D.W.W.; Visualization: M.A.G., L.A.S., D.W.W.; Supervision: D.W.W.; Funding Acquisition: D.W.W.

**Declaration of Interests:** The authors declare no competing interests.

367 **References**


368 Berridge, K.C. (2019). Affective valence in the brain: modules or modes? Nat. Rev. Neurosci.
369 *20*, 225–234.

370 Berridge, K.C., and Aldridge, J.W. (2008). Decision utility, the brain, and pursuit of hedonic
371 goals. Soc. Cogn. *26*, 621–646.

372 Berridge, K.C., and Kringelbach, M.L. (2015). Pleasure systems in the brain. Neuron *86*, 646–
373 664.

374 Betley, J.N., Xu, S., Cao, Z.F.H., Gong, R., Magnus, C.J., Yu, Y., and Sternson, S.M. (2015).
375 Neurons for hunger and thirst transmit a negative-valence teaching signal. Nature *521*, 180.

376 Calu, D.J., Roesch, M.R., Stalnaker, T.A., and Schoenbaum, G. (2007). Associative Encoding in
377 Posterior Piriform Cortex during Odor Discrimination and Reversal Learning. Cereb Cortex *17*,
378 1342–1349.

379 Carlezon, W.A., and Chartoff, E.H. (2007). Intracranial self-stimulation (ICSS) in rodents to
380 study the neurobiology of motivation. Nat. Protoc. *2*, 2987–2995.

381 Chen, T.-W., Wardill, T.J., Sun, Y., Pulver, S.R., Renninger, S.L., Baohan, A., Schreiter, E.R.,
382 Kerr, R.A., Orger, M.B., Jayaraman, V., et al. (2013). Ultrasensitive fluorescent proteins for
383 imaging neuronal activity. Nature *499*, 295–300.

384 Chikazoe, J., Lee, D.H., Kriegeskorte, N., and Anderson, A.K. (2014). Population coding of
385 affect across stimuli, modalities and individuals. Nat Neurosci *17*, 1114–1122.

386 Cohen, J.Y., Haesler, S., Vong, L., Lowell, B.B., and Uchida, N. (2012). Neuron-type-specific
387 signals for reward and punishment in the ventral tegmental area. Nature *482*, 85–88.

388 Doucette, W., Gire, D.H., Whitesell, J., Carmean, V., Lucero, M.T., and Restrepo, D. (2011).
389 Associative Cortex Features in the First Olfactory Brain Relay Station. Neuron *69*, 1176–1187.

390 Gadziola, M.A., and Wesson, D.W. (2016). The Neural Representation of Goal-Directed Actions
391 and Outcomes in the Ventral Striatum's Olfactory Tubercle. J. Neurosci. *36*, 548–560.

392 Gadziola, M.A., Tylicki, K.A., Christian, D.L., and Wesson, D.W. (2015). The Olfactory Tubercle
393 Encodes Odor Valence in Behaving Mice. J. Neurosci. *35*, 4515–4527.

394 Gire, D.H., Whitesell, J.D., Doucette, W., and Restrepo, D. (2013). Information for decision-
395 making and stimulus identification is multiplexed in sensory cortex. Nat Neurosci *16*, 991–993.

396 Gong, S., Zheng, C., Doughty, M.L., Losos, K., Didkovsky, N., Schambra, U.B., Nowak, N.J.,
397 Joyner, A., Leblanc, G., Hatten, M.E., et al. (2003). A gene expression atlas of the central
398 nervous system based on bacterial artificial chromosomes. Nature *425*, 917–925.

399 Gore, F., Schwartz, E.C., Brangers, B.C., Aladi, S., Stujenske, J.M., Likhtik, E., Russo, M.J.,
400 Gordon, J.A., Salzman, C.D., and Axel, R. (2015). Neural Representations of Unconditioned
401 Stimuli in Basolateral Amygdala Mediate Innate and Learned Responses. Cell *162*, 134–145.

402 Gottfried, J.A. (2009). Olfaction and Its Pleasures: Human Neuroimaging Perspectives. In
403 Pleasures of the Brain, M.L. Kringelbach, and K.C. Berridge, eds. (Oxford University Press), pp.
404 125–145.

405 Gottfried, J.A. (2010). Central mechanisms of odour object perception. Nat Rev Neurosci *11*,
406 628–641.

407 Green, D.M., and Swets, J.A. (1966). Signal detection theory and psychophysics (New York:
408 Wiley).

409 Gunaydin, L.A., Grosenick, L., Finkelstein, J.C., Kauvar, I. V., Fenno, L.E., Adhikari, A.,
410 Lammel, S., Mirzabekov, J.J., Airan, R.D., Zalocusky, K.A., et al. (2014). Natural Neural
411 Projection Dynamics Underlying Social Behavior. Cell *157*, 1535–1551.

412 Heimer, L., Switzer, R.D., and Van Hoesen, G.W. (1982). Ventral striatum and ventral pallidum:
413 Components of the motor system? Trends Neurosci. *5*, 83–87.

414 Hickey, C., and Peelen, M.V. (2015). Neural Mechanisms of Incentive Salience in Naturalistic
415 Human Vision. Neuron *85*, 512–518.

416 Ikemoto, S. (2003). Involvement of the Olfactory Tubercle in Cocaine Reward: Intracranial Self-
417 Administration Studies. J. Neurosci. *23*, 9305–9311.

418 Ikemoto, S. (2007). Dopamine reward circuitry: Two projection systems from the ventral
419 midbrain to the nucleus accumbens-olfactory tubercle complex. Brain Res Rev *56*, 27–78.

420 Ilango, A., Kesner, A.J., Keller, K.L., Stuber, G.D., Bonci, A., and Ikemoto, S. (2014). Similar
421 Roles of Substantia Nigra and Ventral Tegmental Dopamine Neurons in Reward and Aversion.

422 J. Neurosci. *34*, 817–822.

423 Isosaka, T., Matsuo, T., Yamaguchi, T., Funabiki, K., Nakanishi, S., Kobayakawa, R., and
424 Kobayakawa, K. (2015). Htr2a-Expressing Cells in the Central Amygdala Control the Hierarchy
425 between Innate and Learned Fear. Cell *163*, 1153–1164.

426 Kermen, F., Midroit, M., Kuczewski, N., Forest, J., Thevenet, M., Sacquet, J., Benetollo, C.,
427 Richard, M., Didier, A., and Mandairon, N. (2016). Topographical representation of odor
428 hedonics in the olfactory bulb. Nat Neurosci *19*, 876–878.

429 Kim, J., Lee, S., Fang, Y.-Y., Shin, A., Park, S., Hashikawa, K., Bhat, S., Kim, D., Sohn, J.-W.,
430 Lin, D., et al. (2019). Rapid, biphasic CRF neuronal responses encode positive and negative
431 valence. Nat. Neurosci. *22*, 576–585.

432 Knaden, M., and Hansson, B.S. (2014). Mapping odor valence in the brain of flies and mice.
433 Curr. Opin. Neurobiol. *24*, 34–38.

434 Kobayakawa, K., Kobayakawa, R., Matsumoto, H., Oka, Y., Imai, T., Ikawa, M., Okabe, M.,
435 Ikeda, T., Itohara, S., Kikusui, T., et al. (2007). Innate versus learned odour processing in the
436 mouse olfactory bulb. Nature *450*, 503–508.

437 Kudo, Y., Akita, K., Nakamura, T., Ogura, A., Makino, T., Tamagawa, A., Ozaki, K., and
438 Miyakawa, A. (1992). A single optical fiber fluorometric device for measurement of intracellular
439 Ca2+ concentration: Its application to hippocampal neurons in vitro and in vivo. Neuroscience
440 *50*, 619–625.

441 Kumar, S., von Kriegstein, K., Friston, K., and Griffiths, T.D. (2012). Features versus Feelings:
442 Dissociable Representations of the Acoustic Features and Valence of Aversive Sounds. J.
443 Neurosci. *32*, 14184–14192.

444 Lewin, K. (1935). A Dynamic Theory of Personality (McGraw-Hill Book Company, Inc.).

445 Li, Q., and Liberles, S.D. (2015). Aversion and attraction through olfaction. Curr. Biol. *25*, R120–
446 R129.

447 Li, H., Pullmann, D., Cho, J.Y., Eid, M., and Jhou, T.C. (2019). Generality and opponency of
448 rostromedial tegmental (RMTg) roles in valence processing. Elife *8*, e41542.

449 Lobo, M.K., and Nestler, E.J. (2011). The Striatal Balancing Act in Drug Addiction: Distinct

450 Roles of Direct and Indirect Pathway Medium Spiny Neurons. Front. Neuroanat. *5*, 41.

451 Miller, S.M., Marcotulli, D., Shen, A., and Zweifel, L.S. (2019). Divergent medial amygdala
452 projections regulate approach–avoidance conflict behavior. Nat. Neurosci. *22*, 565–575.

453 Morrison, S.E., and Salzman, C.D. (2009). The Convergence of Information about Rewarding
454 and Aversive Stimuli in Single Neurons. J. Neurosci. *29*, 11471–11483.

455 Murata, K., Kanno, M., Ieki, N., Mori, K., and Yamaguchi, M. (2015). Mapping of Learned Odor-
456 Induced Motivated Behaviors in the Mouse Olfactory Tubercle. J. Neurosci. *35*, 10581–10599.

457 De Olmos, J.S., and Heimer, L. (1999). The Concepts of the Ventral Striatopallidal System and
458 Extended Amygdala. Ann. N. Y. Acad. Sci. *877*, 1–32.

459 Paxinos, G., and Franklin, K. (2000). The Mouse Brain in Stereotaxic Coordinates (San Diego:
460 Academic Press).

461 Pessoa, L., and Adolphs, R. (2010). Emotion processing and the amygdala: from a “low road” to
462 “many roads” of evaluating biological significance. Nat Rev Neurosci *11*, 773–783.

463 Roesch, M.R., Stalnaker, T.A., and Schoenbaum, G. (2007). Associative encoding in anterior
464 piriform cortex versus orbitofrontal cortex during odor discrimination and reversal learning.
465 Cereb Cortex *17*, 643–652.

466 Schoenbaum, G., and Eichenbaum, H. (1995). Information coding in the rodent prefrontal
467 cortex. I. Single-neuron activity in orbitofrontal cortex compared with that in pyriform cortex. J
468 Neurophysiol *74*, 733–750.

469 Schoenbaum, G., Chiba, A.A., and Gallagher, M. (1998). Orbitofrontal cortex and basolateral
470 amygdala encode expected outcomes during learning. Nat Neurosci *1*, 155–159.

471 Schoenbaum, G., Setlow, B., Saddoris, M.P., and Gallagher, M. (2003). Encoding predicted
472 outcome and acquired value in orbitofrontal cortex during cue sampling depends upon input
473 from basolateral amygdala. Neuron *39*, 855–867.

474 Soares-Cunha, C., Coimbra, B., Sousa, N., and Rodrigues, A.J. (2016). Reappraising striatal
475 D1- and D2-neurons in reward and aversion. Neurosci. Biobehav. Rev. *68*, 370–386.

476 Thompson, K.G., Hanes, D.P., Bichot, N.P., and Schall, J.D. (1996). Perceptual and motor

477 processing stages identified in the activity of macaque frontal eye field neurons during visual
478 search. J. Neurophysiol. *76*, 4040–4055.

479 Tolman, E. (1932). Purposive Behavior (New York: Appleton-Century).

480 Veit, L., and Nieder, A. (2013). Abstract rule neurons in the endbrain support intelligent
481 behaviour in corvid songbirds. Nat Commun *4*, 2878.

482 Veldhuizen, M.G., Rudenga, K.J., and Small, D.M. (2009). The pleasure of taste, flavor, and
483 food. In Pleasures of the Brain, M.L. Kringelbach, and K.C. Berridge, eds. (Oxford University
484 Press), pp. 146–168.

485 Verhagen, J. V, Wesson, D.W., Netoff, T.I., White, J.A., and Wachowiak, M. (2007). Sniffing
486 controls an adaptive filter of sensory input to the olfactory bulb. Nat Neurosci *10*, 631–639.

487 Vicente, A.M., Galvão-Ferreira, P., Tecuapetla, F., and Costa, R.M. (2016). Direct and indirect
488 dorsolateral striatum pathways reinforce different action strategies. Curr. Biol. *26*, R267–R269.

489 Voorn, P., Jorritsma-Byham, B., Van Dijk, C., and Buijs, R.M. (1986). The dopaminergic
490 innervation of the ventral striatum in the rat: A light- and electron-microscopical study with
491 antibodies against dopamine. J. Comp. Neurol. *251*, 84–99.

492 Wesson, D.W., and Wilson, D.A. (2011). Sniffing out the contributions of the olfactory tubercle to
493 the sense of smell: hedonics, sensory integration, and more? Neurosci Biobehav Rev *35*, 655–
494 668.

495 Wilson, D.A., and Sullivan, R.M. (2011). Cortical processing of odor objects. Neuron *72*, 506–
496 519.

497 Wilson, D.A., Sullivan, R.M., and Leon, M. (1987). Single-unit analysis of postnatal olfactory
498 learning: modified olfactory bulb output response patterns to learned attractive odors. J
499 Neurosci *7*, 3154–3162.

500 Zhang, Z., Zhang, H., Wen, P., Zhu, X., Wang, L., Liu, Q., Wang, J., He, X., Wang, H., and Xu,
501 F. (2017a). Whole-Brain Mapping of the Inputs and Outputs of the Medial Part of the Olfactory
502 Tubercle. Front. Neural Circuits *11*, 52.

503 Zhang, Z., Liu, Q., Wen, P., Zhang, J., Rao, X., Zhou, Z., Zhang, H., He, X., Li, J., Zhou, Z., et
504 al. (2017b). Activation of the dopaminergic pathway from VTA to the medial olfactory tubercle

generates odor-preference and reward. Elife *6*.

527 **Figure Legends**

528 **Figure 1. Paradigm for investigating the distribution of odor valence encoding among**
529 **olfactory cortices. A)** Recording schematic indicating simultaneous monitoring of OT and pPCX
530 activity with multi-channel arrays in mice (8 wires/region). pPCX and OT activity were recorded
531 on opposite hemispheres within mice. **B)** Schematic of head-fixed behavioral set-up and **C)**
532 experimental trial outline. Water-deprived mice implanted with chronic multi-site arrays into their
533 OT and pPCX (as in A) and a head-bar were acclimated to head restraint and shaped in a lick/no-
534 lick odor discrimination task wherein following a variable inter-trial interval (ITI) one odor signaled
535 the availability of a small palatable fluid reward from a reward spout following odor offset (during
536 the 'lick reward available' epoch). Alternative (unreinforced) odors were conditioned to not signal
537 reward availability. OT and pPCX unit activity was acquired throughout performance in the task.
538 **D)** Example OT and pPCX unit activity indicating odor valence encoding by neurons in both
539 structures. Multiunit activity (MUA) was spike sorted off-line to identify single-unit activity (SUA)
540 using template matching and cluster cutting with principal component analyses. Vertical lines on
541 the lick trace indicate timing of individual licks (detected with an infrared photo-beam in front of
542 the lick spout). Vertical scale bar applies to both OT and pPCX MUA channels. Data are from two
543 consecutive trials.

544 **Figure 2. OT neurons display greater divergent responses to conditioned odors than pPCX.**
545 **A**) Time course of odor-evoked changes in firing rate relative to baseline as indicated by auROC
546 in response to unrewarded and rewarded odors in the pPCX (left; n=70 neurons) and OT (right;
547 n=104 neurons). Each row represents one single responsive neuron, and neurons are sorted by
548 baseline rates during rewarded odor trials (top row = lowest rate). **B**) Population average auROC
549 values for all responsive neurons in response to rewarded and unrewarded odors compared
550 against a shuffled control distribution. Both regions show an increase in auROC values >0.5
551 shortly after odor onset, indicating increases in firing relative to baseline. Across the population,
552 OT neurons displayed more divergent responses to conditioned odors than pPCX neurons, with
553 the rewarded odor eliciting larger and more persistent changes to firing rate relative to the
554 unrewarded odor. Population values represent the mean ± SEM.

555 **Figure 3. D1-type medium spiny neurons underlie odor valance coding in the OT. A)**
556 Example localization of an optical fiber implant into a mouse injected with GCamP6f (green). The
557 optical fiber was positioned to terminate immediately dorsal to the OT. **B)** Schematic of the fiber
558 photometry system for use in head-fixed behaving mice. 465nm and 405nm LEDs excitation

559 wavelengths passed through dichroic mirrors prior to being sent into the implanted optical fiber
560 via a patch cable. GCaMP6f and UF emission were then both amplified by femtowatt
561 photoreceivers prior to being digitized simultaneously with behavioral data and stimulus
562 presentation events. Please see Fig 1 for a description of the head-fixed paradigm. Example
563 GCaMP6f responses to the original rewarded and unrewarded odors in a single D1-Cre **(C)** and
564 D2-Cre mouse **(D)** averaged over 10 trials of correct behavioral responses during blocks of
565 criterion behavioral performance. These example averaged traces indicate divergent responses
566 to the original rewarded odor vs the original unrewarded odor in D1-Cre but not D2-Cre mice,
567 which is maintained at the population level when averaging across 5 mice, throughout 2-3
568 sessions during criterion behavioral performance (**E & F**). The encoding of odor valence in D1-
569 Cre mice (as in **E**) was confirmed in experiments wherein the odor-reward contingencies were
570 reversed (original rewarded = no unrewarded, and vice versa) (**G & H**). Insets in **G & H** display
571 the mean delta f/f during 0.5-0.75sec of odor in for all four stimulus types. ***=$p$<0.001. ns = not
572 significant ($p$>0.05). no significance was found in any planned comparison in the D2-Cre mice
573 (**H**).

574 **Figure 4**. **D1-type OT medium spiny neurons promote reinforcement and approach**
575 **behaviors. (A)** Example expression of channelrhodopsin2 (ChR2) in OT D1-type MSNs. **(B)**
576 Optogenetic intracranial self-stimulation (opto-ICSS) task schematic wherein mice were required
577 to nose poke in exchange for blue-light mediated optogenetic excitation of OT D1-MSNs. At least
578 2 weeks following injection with either a floxed AAV encoding ChR2 and a reporter fluorophore
579 (AAV.ChR2) or a floxed AAV solely encoding a reporter fluorophore (AAV), mice were shaped on
580 the opto-ICSS task. Please see text for a description of the four task phases. **(C)** Pie chart
581 indicating that all but one AAV.ChR2 mouse reached criterion performance on phase 1 of the
582 task. **(Di)** Performance of two example mice during phases 2-4 of the opto-ICSS task. The mice
583 displayed diversity in their number of pokes into the active port, and in their % of pokes displayed
584 for the active (blue-light emitting) versus inactive ports. Both of these mice reached criterion on
585 phase 2 and phase 3 wherein they had to learn to redirect their poking for a new active port
586 location (reversal learning). Shown also is the behavior of these two mice during extinction,
587 wherein the port lights were on (viz., both ports were visually 'active') but no optogenetic
588 stimulation was available regardless of poking. **(Dii)** A win-loss plot for mouse 127 from session
589 2-5. **(E)** Quantification of opto-ICSS data indicating that ChR2 mediated stimulation of OT D1-
590 MSNs promotes reinforcement and approach behaviors. The first phase of reversal learning

591 resulted in a significant reduction in % pokes for the new active port, which with experience was
592 restored on the last session of the reversal phase.

593

594

595

596 **Supplementary Figure Legends**

597 **Supplementary Figure 1. A)** Histological verification of pPCX and OT recording sites. **B)**
598 Background firing rate distribution of all pPCX and OT single-units used for analysis. **C)** Summary
599 of learning and performance in the lick/no-lick odor discrimination task for mice contributing single-
600 unit data. Red dashed horizontal line = criterion behavioral performance level.

601 **Supplementary Figure 2.** Time course of odor-evoked changes in firing rate separated by
602 response type. Population average auROC values for all responsive neurons in PCX and OT
603 (same neurons as in Fig. 2), separated by whether the response was excited or suppressed
604 relative to baseline. Population values represent the mean ± SEM.

605 **Supplementary Figure 3. A)** Histological verification of optical fiber implants from all mice
606 contributing fiber photometry data. Summary of learning and performance in the lick/no-lick odor
607 discrimination task for D1-Cre **(B)** and D2-Cre mice **(C)** contributing fiber photometry data. Red
608 dashed horizontal line = criterion behavioral performance level.

609 **Supplementary Figure 4. A)** Histological verification of optical fiber implants from mice
610 contributing optical-intracranial self-stimulation data (opto-ICSS).

611

612

613

614

615

616

617

618 **Methods**

619 *Animals.* Eleven 2-4 months of age male C57bl/6 mice originating from Harlan Laboratories
620 (Indianapolis, IN) were used for single-unit recordings. For fiber photometry, we utilized male
621 bacterial artificial chromosome transgenic mice expressing Cre-recombinase under control of the
622 *drd1a* (D1-Cre; *n* = 7; obtained from the UC Davis Mutant Mouse Regional Resource Center,
623 strain EY262Gsat/Mmucd) or *drd2* gene (D2-Cre; *n* = 7; obtained from the UC Davis Mutant
624 Mouse Regional Resource Center, strain ER44Gsat)(Gong et al., 2003). Genotyping was
625 performed following standard protocols using tail tissue DNA. Mice were housed on a 12:12 h
626 light-dark cycle with food and water available *ad libitum*, except when water was restricted for
627 behavioral training (see below). Up to 5 mice were co-housed in a cage before experimentation,
628 but all post-surgical animals were housed individually. All experimental procedures were
629 conducted in accordance with the guidelines of the National Institutes of Health and were
630 approved by the Case Western Reserve University and University of Florida Institutional Animal
631 Care and Use Committees.

632

633 *Methods for multi-site single-unit recordings during lick/no-lick odor discriminations.*

634 Surgical procedures were conducted as described previously (Gadziola et al., 2015; Gadziola &
635 Wesson, 2016). Briefly, mice were anesthetized with Isoflurane (2-4% in oxygen, Abbott
636 Laboratories, Green Oaks, IL), and mounted in a stereotaxic frame with a water-filled heating pad
637 (38°C) beneath to maintain body temperature. An injection of a local anesthetic (0.05% marcaine,
638 0.1 ml s.c.) was administered before exposing the dorsal skull. A craniotomy was made to access
639 the OT and pPCX, each contralateral from another (see **Fig S1A** for distribution). An 8-channel
640 micro-wire electrode array (PFA-insulated tungsten wire, with four electrode wires encased
641 together in a 254 μm diameter polyimide tube (Gadziola et al., 2015)) was implanted within the
642 OT (4.9 mm ventral) and posterior PCX (4.2 mm ventral) (**Fig 1A and S1A**), and cemented in
643 place, along with a headbar for later head fixation. The hemisphere receiving an array into each
644 structure was not held constant across animals but instead varied (**Fig S1A**). Additional
645 craniotomies were drilled over a single neocortex for placement of a stainless steel ground wire.
646 During a three-day recovery period, animals received a daily injection of carprofen (5 mg/kg, s.c.,
647 Pfizer Animal Health, New York, NY) or meloxicam (5mg/kg; Putney, Inc., Portland, ME) and *ad*
648 *libitum* access to food and water. Animals were allowed 5-7 days for post-op recovery before
649 beginning water restriction.

650

651

652 *Olfactory lick/no-lick odor discrimination and reversal learning behavioral task.* Mice were mildly
653 water-restricted for three days prior to behavioral training. Bodyweight was monitored daily and
654 maintained at 85% of their original weight. Mice were trained in cohorts of three to four. All
655 behavioral procedures were performed during the light hours, in a dim room. Head-fixed mice
656 were trained in a lick/no-lick odor discrimination task (**Fig 1C**) across multiple 1 hour recording
657 sessions in which the mice obtained a fluid reward for licking a spout positioned in front of their
658 snouts in trials with reinforced odors (Gadziola et al., 2015), adapted from (Verhagen et al., 2007).
659
660 Licking was measured by a pair of infrared photo-beams positioned to cross in front of the lick
661 spout by ~2 mm. Mice were first trained to lick the water spout for reward, with a progressively
662 increasing inter-trial interval (ITI) (3 ± 1 s, Phase 1). In Phase 2, odor presentation began with a
663 10 ± 2 s ITI, and mice were only rewarded for licking during a 2 s period after odor offset (FR1).
664 Licking during the odor was discouraged by moving the lick spout further away from the snout. In
665 Phase 3, trials were randomized between rewarded and unrewarded trials (17 ± 2 sec ITI); for
666 unrewarded odor trials, mice were presented with a “blank” stimulus (mineral oil) and had to learn
667 to withhold licking during these trials. Finally, in Phase 4, trials (17 ± 2 s ITI) were randomized
668 between the rewarded and unrewarded odors. In go trials, mice would receive a reward for licking
669 a spout within 2sec following the offset of the rewarded odor (hit); not licking would be considered
670 a miss. In no-go trials, mice were presented with an unreinforced odor and did not receive a water
671 reward regardless of whether they licked (false alarm) or correctly withheld licking for the total
672 odor duration of the trial (correct reject). Next, mice continued on Phase 5 to learn a novel odor
673 pair. Phase 5 consisted of pseudo-random trials (17 ± 2 s ITI) among which all four odors were
674 separately presented, with the two reinforced odors both resulting in a low-value reward. Finally,
675 in Phase 6, the four odors were presented (17 ± 2 s ITI), with one rewarded odor being assign to
676 the high value saccharine and the other to the low value saccharine. Mice discriminated among
677 the four odors, two of which predicted presentation of reward (either low or high value saccharine),
678 and two unrewarded odors. These sessions include the original training odor set, as well as novel
679 odors presented on a different experimental day (each mouse was shaped on 2 novel sets of four
680 odors on different sessions). No major effects were observed between high versus low value
681 rewarded odor evoked responses nor behavior and therefore herein any odors paired with
682 reinforcers are classified as conditioned rewarded odors, whereas those not paired are termed
683 conditioned unrewarded odors. Throughout all phases, behavioral performance was evaluated in
684 blocks of 20 trials, and mice were required to achieve a performance criterion ≥80% correct for
685 two consecutive blocks in order to advance to the next phase. Neural activity was recorded

686 throughout all training phases, but analysis of odor-evoked activity was restricted to post-training
687 sessions.
688
689 *Stimulus Delivery.* Odors were presented through a custom air-dilution olfactometer with
690 independent stimulus lines up to the point of entry into the odor port. In addition to a blank stimulus
691 (mineral oil), odors included ethyl butyrate, 1,7-octadiene, isopentyl acetate, heptanal, 2-
692 heptanone, (+)-limonene, ethyl propionate, (-)-limonene, methanol, methyl valerate, 2-butanone,
693 1,4-cineole, butanal, propyl acetate, allylbenzene, allyl bromide, isobutyl propionate, and 2-
694 methylbutyraldehyde (Sigma Aldrich, St. Louis, MO; all >97% purity). These molecularly diverse
695 odors were diluted in their liquid state to 1 Torr (133.32 Pa) in mineral oil and were then further
696 diluted to 10% (vol/vol) by mixing 100 ml odor vaporized $N_2$ with 900 ml medical grade $N_2$ (Airgas,
697 Radnor, PA). Thus, stimuli were delivered at a total flow rate of 1 L/min. Not all animals were
698 tested with all odors. The rewarded and unrewarded odor pairs were pseudo-randomly assigned
699 to each cohort prior to training (neurons were not initially screened for odor responsiveness). The
700 experimenter was not blind to odor assignment, but all stimulus presentation was automated.
701 Presentation of rewarded and unrewarded odors were pseudo-randomized within each block,
702 delivered for 2 s duration with a 17 ± 2 s ITI through a Teflon odor-port (9 mm diameter opening)
703 directed towards the animal's snout at a distance of 1 cm. Odor was continuously flowing to the
704 odor-port but was removed by a vacuum before exiting towards the animal. Recordings with a
705 photoionization detector (miniPID, Aurora Scientific, Ontario, Canada) were used to confirm the
706 temporal dynamics of the odor presentation in this design. While the dynamics may vary slightly
707 across odors, they confirm the precision and stability of the odor presentation methods used in
708 this study.
709
710 *Reward Delivery.* Reward fluids were delivered through a custom 3D-printed polylactic acid lick
711 spout, as reported previously (Gadziola and Wesson, 2016). Independent stimulus lines
712 terminated onto 20G blunted needles that passed through one of seven 1-mm holes and extended
713 to the tip of the spout. In the current task, two adjacent holes on the lick spout were used for
714 reward delivery, three were connected to a vacuum line, and the last two unused holes were
715 blocked. Animals were reinforced with a 4μL drop of 2-20mM saccharin (Sigma Aldrich, St. Louis,
716 MO; dissolved in water). Reward volumes were calibrated for the individual reward valves.
717
718 *In vivo Electrophysiology.* The outputs of the electrode arrays were amplified, digitized at 24.4
719 kHz, filtered (bandpass 300-5000 Hz), and monitored (Tucker-Davis Technologies, Alachua, FL),

720 along with licking (300 Hz sampling rate), and odor and reward presentation events. One
721 electrode wire was selected to serve as a local reference for each headstage. Our electrode
722 arrays were fixed in place and no attempt was made to record from unique populations of neurons
723 on different sessions. To compensate for the possibility that the same neurons were recorded
724 across multiple days, two different behavioral tasks were employed and statistical comparisons
725 are only made within each task type. Sessions of the same task and odor pair were run for 1-3
726 consecutive days to achieve adequate behavioral performance and/or capture the dynamics of
727 newly identified neurons. On average, 3.5 ± 1.9 single neurons were identified per mouse per
728 session (range: 1-7 neurons), with an average of 1.4 ± 0.6 neurons recorded per viable electrode
729 wire per mouse per session (range: 1-3 neurons). Numbers were comparable when separated by
730 region (± 0.1 single units / region difference).

731

732 *Analysis of odor-evoked electrophysiology data.* Single neurons were sorted offline in Spike2
733 (Cambridge Electronic Design, Cambridge, England), using a combination of template matching
734 and cluster cutting based on principle component analysis. Single neurons were further defined
735 as having <2% of the spikes occurring within a refractory period of 2 ms. Spike times associated
736 with each trial were extracted and exported to MATLAB (Mathworks, Natick, MA) for further
737 analysis. To examine modulations in firing rate within a single trial, spike density functions were
738 calculated by convolving spike trains with a function resembling a postsynaptic potential
739 (Thompson et al., 1996). Mean firing rates across trials were measured in 50 ms bins, along with
740 the 95% confidence interval. Mean baseline firing rate for each neuron was averaged across a 2
741 s period prior to odor onset.

742 Animals were typically presented with at least 40 trials of each rewarded and unrewarded
743 odor set per session. To ensure that animals were engaged in the task, only blocks possessing
744 high behavioral performance were analyzed. On some trials, mice may have been licking during
745 odor presentation. Any trials in which the animal licked during the first 1.5s period after odor onset
746 were removed. This ensured that any odor-evoked activity observed during the first several
747 hundred ms was not due to licking-related activity. Of the 11 animals with bilateral implants, 10
748 were confirmed to reside within the OT and 8 within the PCX. One of the 10 OT-confirmed animals
749 did not contribute data since they did not yield well-isolated neurons. From all mice contributing
750 data, 7 yielded simultaneous OT and PCX single-units.

751

752 *ROC Analysis.* The area under the receiver operating characteristic (auROC) is a nonparametric
753 measure of the discriminability of two distributions (Green and Swets, 1966). To normalize activity
754 across neurons, we used an auROC method that quantifies stimulus-related changes in firing rate
755 to the baseline activity on a 0-1 scale (for more details see (Cohen et al., 2012)). A value of 0.5
756 indicates completely overlapping distributions, whereas values of 0 or 1 signal perfect
757 discriminability. We calculated the auROC at each 50-ms time bin over a 4 s period centered on
758 stimulus onset for each neuron. Values greater than 0.5 indicate the probability that firing rates
759 were increased relative to the pre-stimulus background (excitation), whereas values less than 0.5
760 indicate the probability that firing rates were decreased relative to the pre-stimulus background
761 (inhibition). Similar trial numbers have been used for calculating auROC (Veit and Nieder, 2013;
762 Gadziola et al., 2015, Gadziola & Wesson, 2016). To obtain mean auROC values, the auROC
763 values of individual neurons were averaged at each time bin. In some cases mean auROC values
764 were computed separately for all excitatory and inhibitory neurons.
765

766 *Methods for fiber photometric-based imaging of D1- and D2-type OT MSNs during lick/no-lick*
767 *odor discrimination and reversal learning.*

768 *Virus injection and optical fiber Implantation.* To achieve cell-type specific GCaMP6f (Chen et al.,
769 2013) expression, D1- and D2-Cre mice were injected with AAV5-EF1a-DIO-GCaMP6f-WPRE
770 ($5.43^{e13}$ GC/ml, obtained from the Penn Vector Core in the Gene Therapy Program of the Univ of
771 Pennsylvania). Stereotaxic surgery was performed as described above with exceptions as noted
772 below. 1µl of virus was infused into the OT at a rate of 0.1nl/sec and allowed to diffuse for 10mins
773 before needle was slowly withdrawn over the subsequent 20mins. This injection paradigm was
774 not intended to infect solely OT neurons, but to yield a bolus of infected cells which could be later
775 targeted selectively for imaging by careful localization of the optical fiber. Following, the
776 craniotomy was sealed with wax and the wound margin closed. Animals were allowed 2 weeks
777 for the virus to transduce and then a 400µm core, 0.48NA optical fiber, threaded through metal
778 ferrules were chronically implanted to terminate within the OT. Implants were cemented in place
779 along with a headbar for later head fixation. As with the single-unit recordings, animals were
780 allowed 5-7 days for post-op recovery before beginning water restriction. D1- and D2-Cre mice
781 were tested in mixed cohorts.
782

783 *Imaging.* 465nm (GCaMP excitation wavelength, driven at 210 Hz) and 405nm (UV excitation
784 wavelength, driven at 330Hz; control channel) light emitting diodes were coupled to a 5 port
785 fluorescence mini cube (FMC5, Doric Lenses) using 400µm core, 0.48NA, 2.5mm FCM optical
786 fiber patchcords. Excitation and emission light were directed through a single optical fiber
787 patchcord connected to the animal via a 2.5mm metal ferrule. Emission light was directed through
788 the 5-port mini cube, and subsequently coupled to a pair of femtowatt photoreceivers (model
789 2151, Newport) for monitoring of the GFP and UV fluorescence. Photometry data were digitized
790 and pulse demodulated at 1kHz, along with the timing of behavioral events (licking) and odor and
791 reward delivery using a Tucker Davis Technologies digital processor (TDT).

792 *Lick/no-lick odor discrimination and reversal learning during photometry.* The methods for
793 operant olfactory behavior employed for fiber photometry were mostly identical to those used
794 for the single-unit recordings (see above) with two exceptions. First, during the fiber photometry
795 imaging, mice were only asked to discriminate between two odors in any given session (one
796 conditioned rewarded and one conditioned unrewarded). Second, mice were shaped in a
797 reversal learning paradigm wherein following reaching successful criterion performance in the
798 original odor discrimination, the contingencies were reversed so that the original rewarded odor
799 no longer signals reinforcement availability (now the 'new unrewarded odor') and the original
800 unrewarded odor now signals reward availability (now the 'new rewarded odor').

801

802 Processing and analysis of photometry data

803 Off-line, the UV signal was subtracted from that of the GFP, filtered (2$^{nd}$ order, 25Hz low-
804 pass), smoothed, and down sampled to 200Hz using a custom script written in Spike2 (Cambridge
805 Electronic Design, Inc). Photometry recordings were normalized across trials off-line, using the
806 mean signal across 3 sec before odor delivery as a trial specific baseline for the ΔF/F values. Of
807 the 7 D1-Cre animals with bilateral implants, 1 was confirmed to have poor/weak viral expression
808 and one have a fiber tip residing outside of the OT. Of the 7 D2-Cre mice, 2 were confirmed to
809 have fiber tips residing outside of the OT. Thus, in total, 5 mice per genotype, which had 1)
810 criterion-level behavioral performance, 2) on target OT fiber tips, and 3) quality viral expression
811 contributed data.
812

813 *Methods for optogenetic stimulation of OT D1 MSNs and intra-cranial self-stimulation.*

814 The surgical methods to allow for expression of ChR2 in OT D1-MSNs are similar to those used
815 for GCaMP6f as described above. Two surgical procedures were performed on each mouse. First,
816 mice were intracranially injected with one of two floxed AAV vectors to allow for expression of
817 AAV5.EF1a.DIO.hChR2(H134R).eYFP or mCherry (to yield optogenetic stimulation) or
818 AAV5.EF1a.DIO.eYFP or mCherry (as control). AAVs were obtained from the University of North
819 Carolina viral vector core. Second, mice were intracranially implanted with a unilateral optic fiber
820 (300um, 0.39NA) into their OT which was attached to a ferrule to allow light transmittance into the
821 brain. AAV injections and ferrule implants occurred in the left hemisphere or right hemisphere to
822 prevent biasing results towards effects which may be lateralized. Using a light meter (Thorlabs,
823 Inc., Newton, New Jersey), all fiber optic implants were verified prior to implantation to deliver 6.5-
824 7.5mW[3] of light energy when using the same LED and LED driver as used during Opto-ICSS
825 testing (see below).
826
827 *Opto-ICSS apparatus and light stimulation*
828 We used a dual nose-poke port apparatus wherein poke into each port is monitored by 880nm
829 infrared photobeams and digitized for later analysis. The floor and three walls of the apparatus
830 were made of black acrylonitrile butadiene styrene (ABS) plastic (30cm tall walls), consisting of a
831 15 x 15cm square floor and a guillotine style ABS door to allow gentle insertion and removal of
832 the mouse from the testing apparatus. One wall of the apparatus was constructed of clear acrylic
833 to allow visual monitoring of the mouse by an experimenter when needed. The ceiling was 'open'
834 to allow for tethering of the animal to an optical rotary joint (Doric Lenses, Inc., Quebec, Canada)
835 which was suspended above the apparatus. The nose-poke ports were 3D-printed out of
836 polylactic acid plastic and were T-shaped with a 2cm opening which faced into the behavioral
837 apparatus to allow nose-entry and monitoring of infrared beam breaks. Photobeam status (open
838 or closed) was acquired continuously and relayed to a PC for data collection using an Arduino
839 microcontroller board running custom code written in the Arduino open source language (Arduino,
840 https://www.arduino.cc). Immediately next to each port was a 3mm white LED, also controlled by
841 the Arduino, which could signal to the mouse active port status (on = active and optical stimulation
842 available, off = inactive and no available optical stimulation).
843 Optogenetic stimulation (25Hz train, 15ms pulse width, 2 sec duration [for opto-ICSS the 2
844 sec stimulation occurred regardless of the nose-poke duration]) was accomplished by means of
845 a 447.5nm LED (Luxeon Rebel ES, Luxeon Stars, Lethbridge, Alberta) driven by a Thorlabs T-
846 Cube LED driver (Thorlabs) and controlled by the digital output of an Arduino microcontroller. This
847 stimulation paradigm was selected following the results of physiological and behavioral pilot

848 studies. An SMA adapter was adhered atop of the LED using optical epoxy to allow for butt
849 coupling of an SMA terminated multimode fiber to the LED. The fiber used to connect the LED to
850 the optic rotary joint as well as the fiber used to connect the rotary joint to the mouse were both
851 300µm core multimode fibers with a 0.39NA (same as the fiber used for the optical implants),
852 encased in 2mm furcation tubing.
853
854 *Opto-ICSS shaping and testing*

855 All behavioral procedures were performed during the light hours, in a dim room. At the start of all
856 sessions, the mice were first gently connected to the fiber optic tether. The mice were then placed
857 into the apparatus and the door closed. The stages of shaping and testing in the opto-ICSS task
858 are illustrated in **Figure 4** and occurred on separate daily 60min sessions. In phase 1, both ports
859 were active (both active port LEDs were on) and nose-poke into either port triggered blue light
860 stimulation. After performing ≥ 40 pokes into either or both ports in a given session, for at least
861 two consecutive sessions, mice were then transitioned into phase 2 of the task. In phase 2, the
862 port wherein the mouse displayed the greatest number of pokes on subsequent days, was set to
863 be active (port LED on, blue light stimulation available) and the alternative port was inactive (port
864 LED off, blue light stimulation unavailable). Only nose poke into the active port triggered light
865 stimulation. After mice reached criterion performance in phase 2 (≥40 pokes, with ≥80% into the
866 active port), they were switched to phase 3 wherein the active and inactive ports were reversed
867 so that the previously inactive port is now the only port which would trigger light stimulation. Phase
868 3 is thus a test of reversal learning and ensures that the animal's tendency to poke is indeed
869 motivated by light-mediated ChR2 stimulation. Those mice which reached criterion performance
870 on phase 3 (see above), were advanced onto phase 4. In all of the previous phases stimulation
871 was available on an FR1 (fixed ratio of 1) schedule. In phase 4, both ports were rendered inactive
872 (both port LEDs were off, blue light off) in a test of extinction. Transitions between phases
873 occurred on subsequent daily testing sessions. Mice which did not reach criterion performance
874 on a given phase by the end of the 6$^{th}$ session of that phase were eliminated from further testing.

875

876 *Histology*

877 Following the end of experiments, mice were overdosed with Fatal-plus (0.01mL/g; Vortech
878 Pharmaceutical, Dearborn, MI) and perfused with 10mL of cold saline followed by 15mL of cold

879 10% phosphate buffered formalin. Brains were stored in 10% formalin/30% sucrose (4ºC) prior to
880 sectioning at 40µm thickness on a Leica sliding microtome. Tissue was later mounted on slides
881 using Fluoromount-G containing DAPI (for fluorescence analysis; 4',6-diamidino-2-phenylindole;
882 Invitrogen, Carlsbad, CA) or stained with 1% cresyl-violet (for tissue contributing single-unit data).
883 Microscopic examination of tissue was conducted on a Nikon Ti2e inverted fluorescent
884 microscope equipped with 5MP color and 15MP monochrome cameras. Histological definition of
885 brain regions was aided by use of a brain atlas (Paxinos and Franklin, 2000).

886

887 *Overall statistical methods*

888 All performed tests were two-sided and met assumptions of normality (Kolmogorov-Smirnov test).
889 Sample sizes are consistent with numbers reported in the field and no statistical method was used
890 to predetermine these. Statistical analyses were performed in SPSS 22.0 (SPSS Inc., Chicago,
891 IL) or MATLAB. All data are reported as mean ± SD unless otherwise noted. Specific details
892 regarding some analytical methods (*e.g.,* ROC) can be found in above sections.

893

# Figure 1

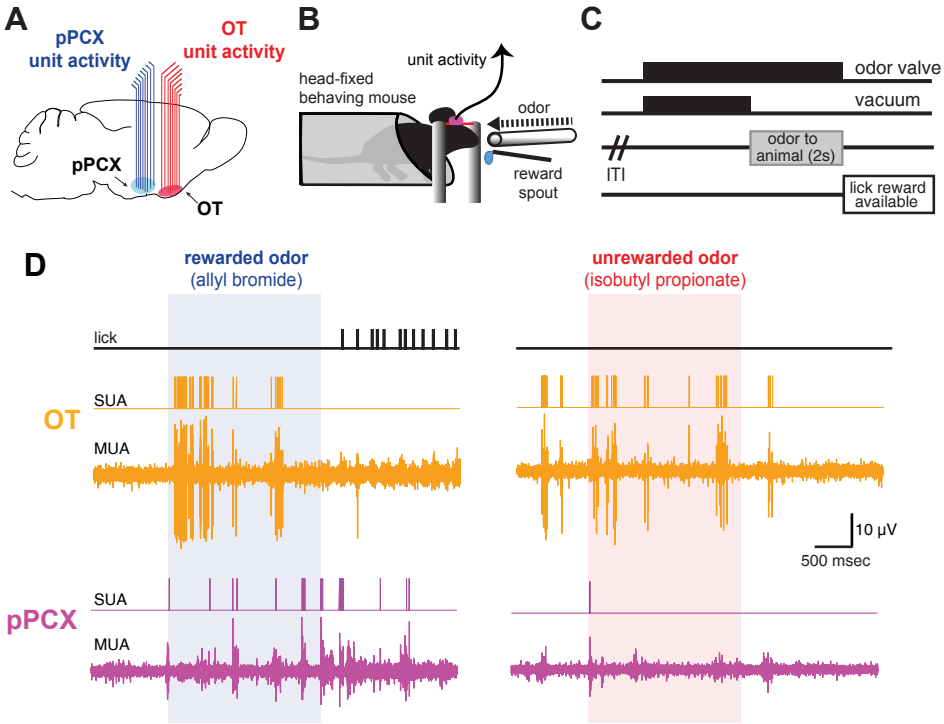
A
pPCX
unit activity
OT
unit activity
pPCX
OT
B
unit activity
head-fixed
behaving mouse
odor
reward
spout
C
odor valve
vacuum
odor to
animal (2s)
ITI
lick reward
available
D
rewarded odor
(allyl bromide)
unrewarded odor
(isobutyl propionate)
lick
OT
SUA
MUA
10 μV
500 msec
pPCX
SUA
MUA

## Figure 2

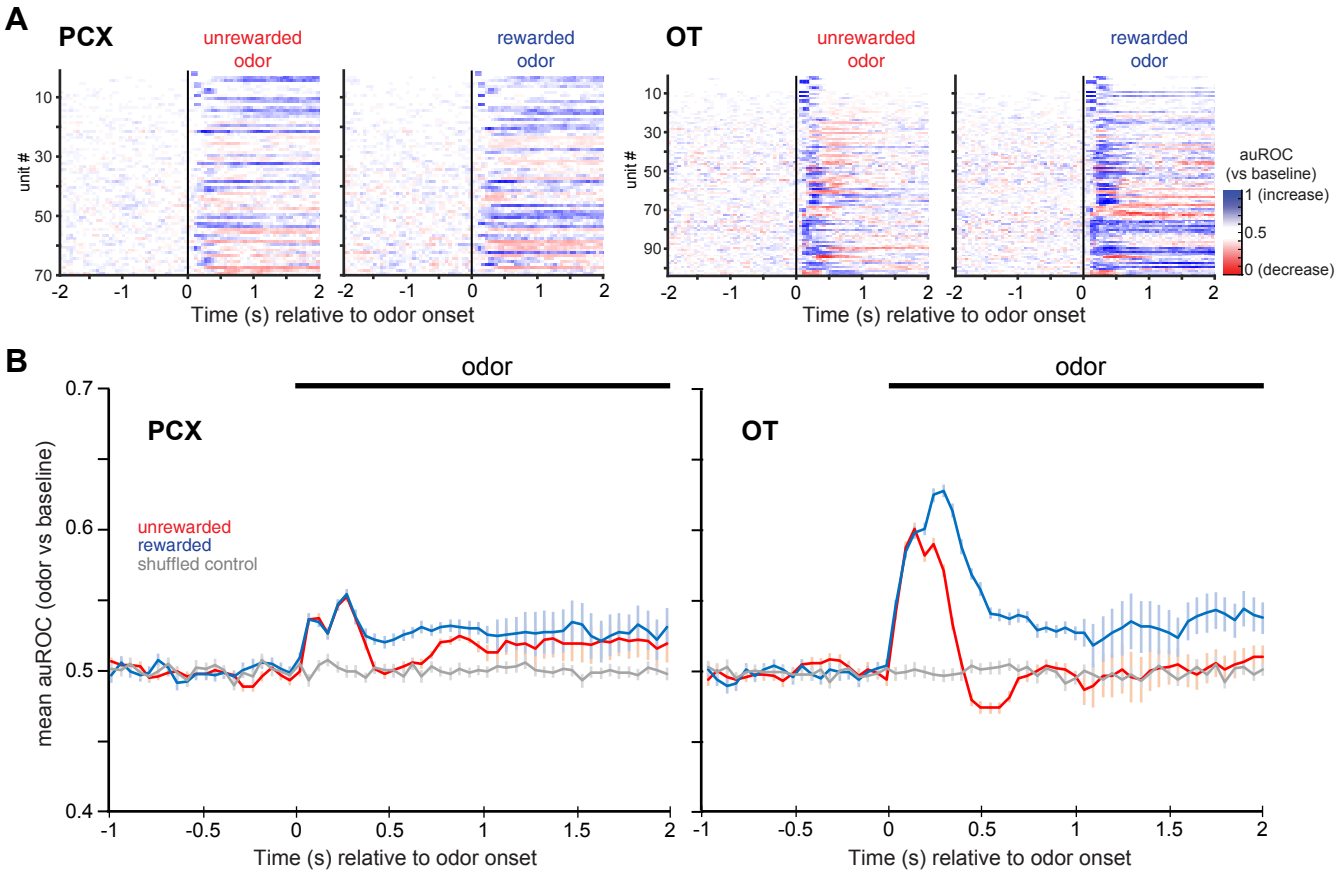
A
PCX
unrewarded odor
rewarded odor
OT
unrewarded odor
rewarded odor
unit #
Time (s) relative to odor onset
auROC (vs baseline)
1 (increase)
0.5
0 (decrease)
B
odor
PCX
OT
unrewarded
rewarded
shuffled control
mean auROC (odor vs baseline)
Time (s) relative to odor onset

# Figure 3

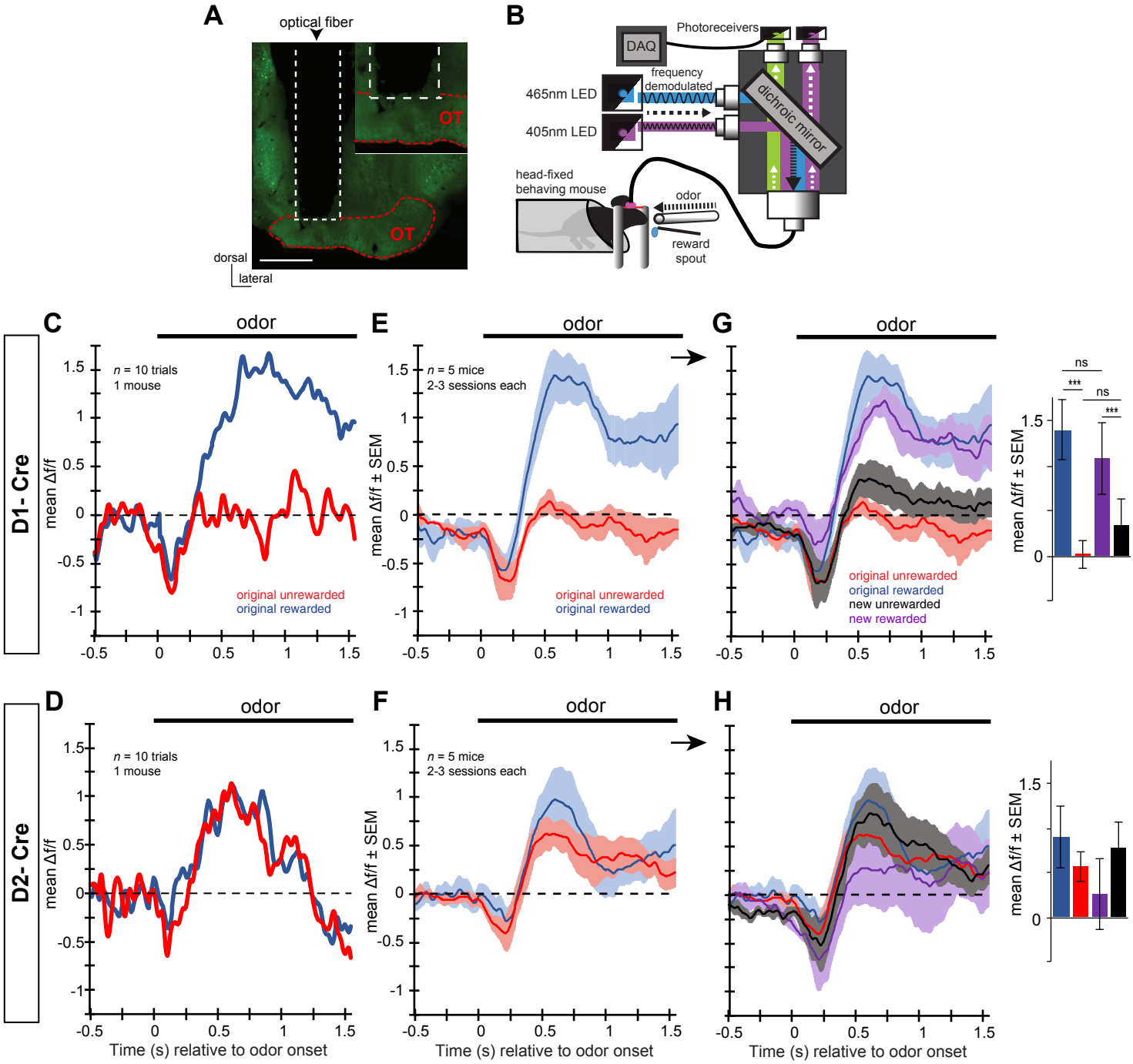
A
optical fiber
OT
OT
dorsal
lateral
B
DAQ
Photoreceivers
frequency demodulated
465nm LED
405nm LED
dichroic mirror
head-fixed behaving mouse
odor
reward spout
D1- Cre
D2- Cre
C
D
E
F
G
H
odor
n = 10 trials
1 mouse
n = 5 mice
2-3 sessions each
mean Δf/f
mean Δf/f ± SEM
original unrewarded
original rewarded
new unrewarded
new rewarded
ns
***
Time (s) relative to odor onset

# Figure 4

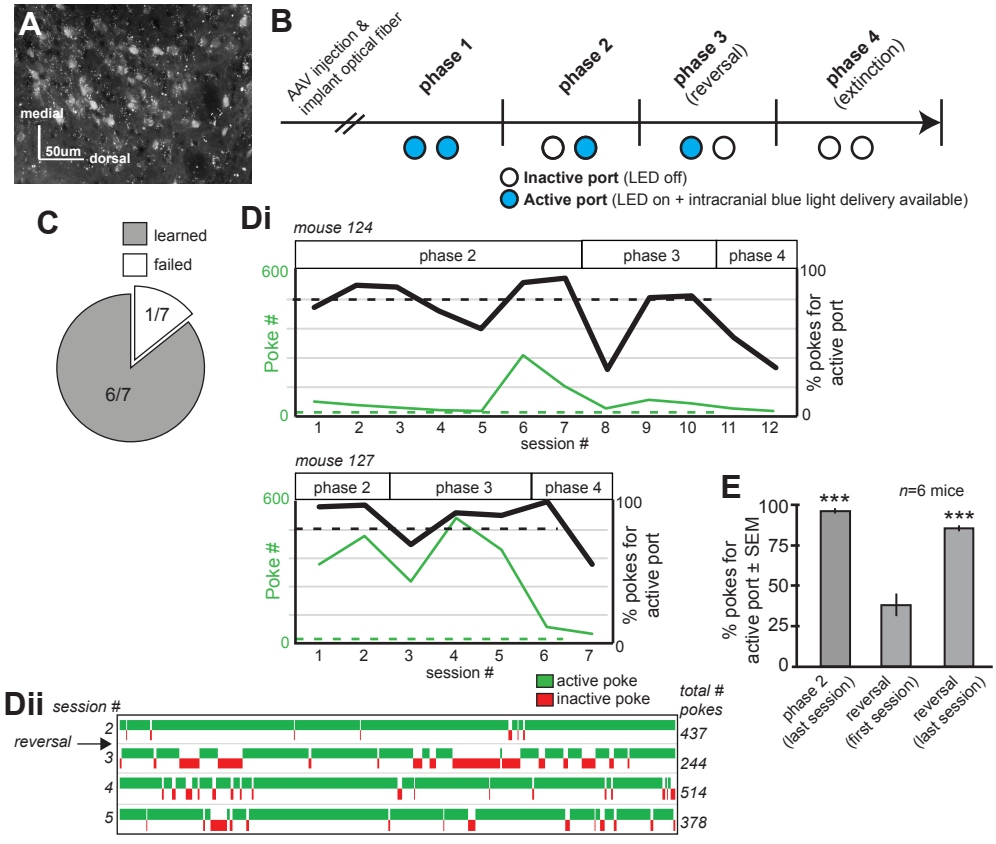
A
medial
50um
dorsal
B
AAV injection & implant optical fiber
phase 1
phase 2
phase 3 (reversal)
phase 4 (extinction)
Inactive port (LED off)
Active port (LED on + intracranial blue light delivery available)
C
learned
failed
1/7
6/7
Di
mouse 124
phase 2
phase 3
phase 4
Poke #
% pokes for active port
session #
mouse 127
active poke
inactive poke
Dii
session #
reversal
total # pokes
437
244
514
378
E
n=6 mice
% pokes for active port ± SEM
phase 2 (last session)
reversal (first session)
reversal (last session)

**Figure S1**

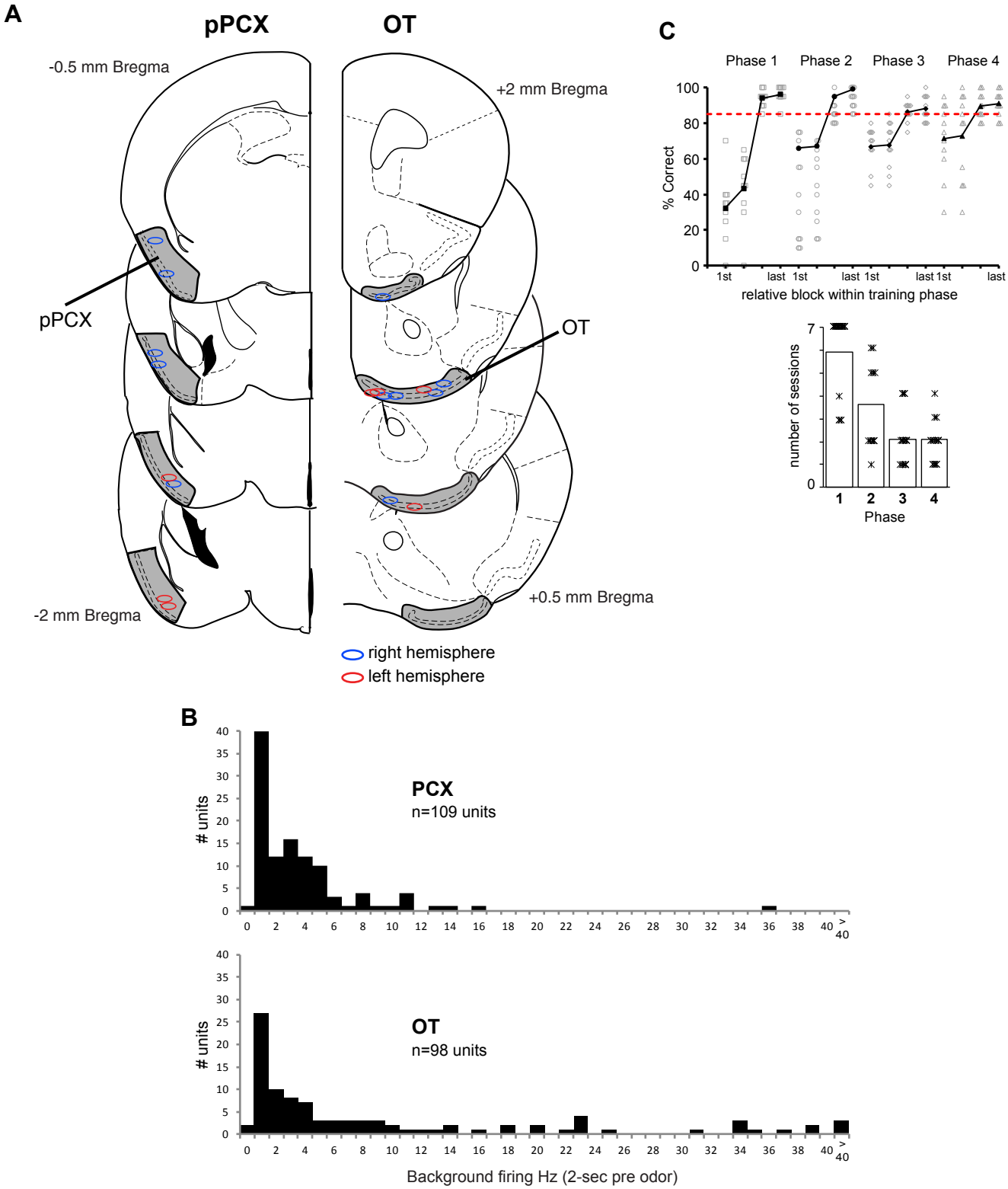
A
pPCX
OT
-0.5 mm Bregma
+2 mm Bregma
pPCX
OT
-2 mm Bregma
+0.5 mm Bregma
right hemisphere
left hemisphere
C
Phase 1
Phase 2
Phase 3
Phase 4
% Correct
relative block within training phase
number of sessions
Phase
B
PCX
n=109 units
OT
n=98 units
# units
Background firing Hz (2-sec pre odor)

## Figure S2

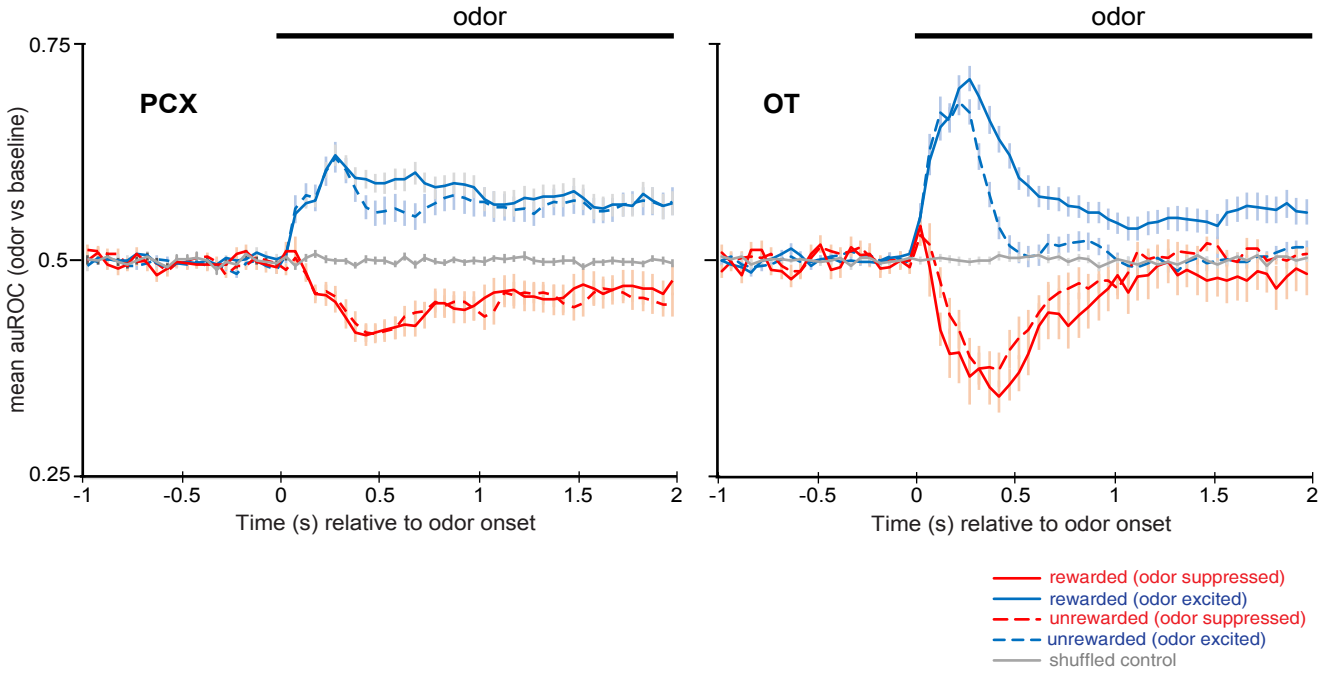
odor
odor
PCX
OT
mean auROC (odor vs baseline)
0.75
0.5
0.25
-1
-0.5
0
0.5
1
1.5
2
Time (s) relative to odor onset
Time (s) relative to odor onset
rewarded (odor suppressed)
rewarded (odor excited)
unrewarded (odor suppressed)
unrewarded (odor excited)
shuffled control

## Figure S3

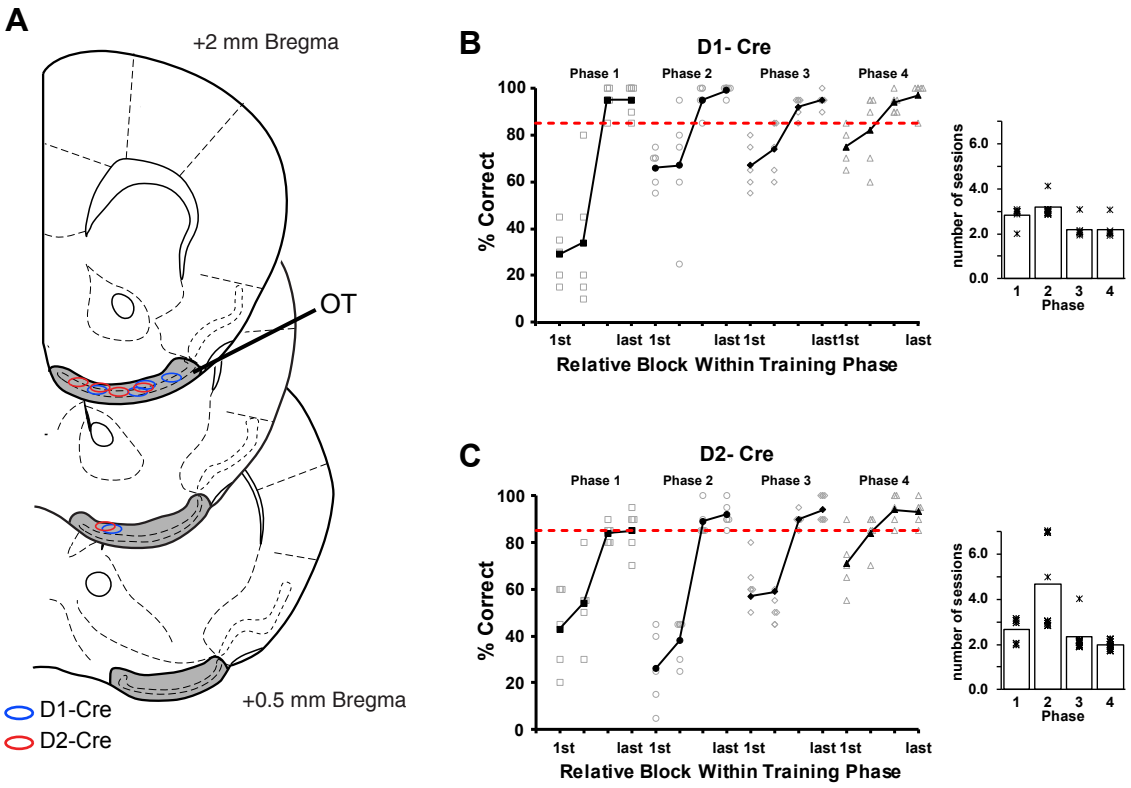
A
+2 mm Bregma
OT
+0.5 mm Bregma
D1-Cre
D2-Cre
B
D1- Cre
Phase 1
Phase 2
Phase 3
Phase 4
% Correct
Relative Block Within Training Phase
1st
last
number of sessions
Phase
C
D2- Cre
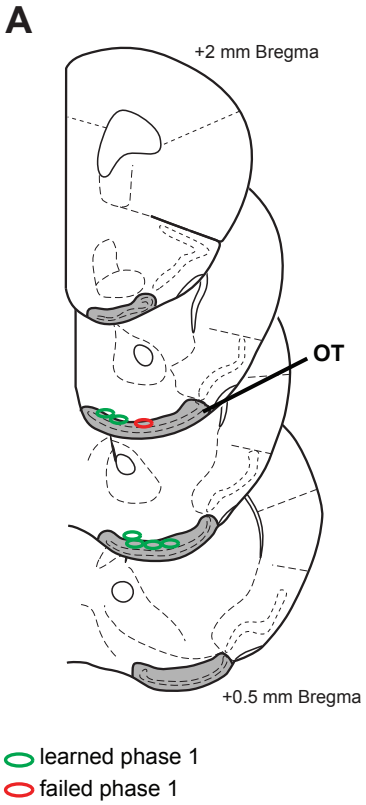
## Figure S4